Journal of Organometallic Chemistry 887 (2019) 32–39

Contents lists available at ScienceDirect

Journal of Organometallic Chemistry

journal homepage: www.elsevier.com/locate/jorganchem

# Luminescent dinuclear rhenium(I)–PNA conjugates for microRNA-21 targeting: Synthesis, chemico-physical and biological characterization

Silvia Cauteruccio [a], Monica Panigati [a, b], Lorenzo Veronese [a], Nadia Zaffaroni [c], Marco Folini [c], Emanuela Licandro [a, *]

[a] Dipartimento di Chimica, Università degli Studi di Milano, via Golgi 19, I-20133, Milan, Italy
[b] Istituto per lo Studio delle Macromolecole, Consiglio Nazionale delle Ricerche (ISMAC-CNR), via A. Corti 12, I-20133, Milan, Italy
[c] Dipartimento di Ricerca Applicata e Sviluppo Tecnologico, Fondazione IRCCS Istituto Nazionale dei Tumori di Milano, via G. A. Amadeo, 42, I-20133, Milan, Italy

ARTICLE INFO

*Article history:*
Received 4 February 2019
Received in revised form
25 February 2019
Accepted 26 February 2019
Available online 4 March 2019

Dedicated to Professor Armando J. L. Pombeiro on the occasion of his 70th birthday

*Keywords:*
Rhenium complex
Peptide nucleic acid
miR-21
Prostate cancer cells
Cell imaging

ABSTRACT

Two different luminescent rhenium complexes, having the general formula $[Re_2(\mu\text{-}Cl)_2(CO)_6(\mu\text{-}1,2\text{-diazine})]$ and containing two different diazine ligands, namely 4-(pyridazin-4-yl)-butanoic acid (**Re-1**) and 8-(5-methylpyridazin-4-yl)-octanoic acid (**Re-2**), were prepared. Exploiting the presence of the carboxylic acid moieties, both complexes were further covalently linked to a 20-mer oligomer (**PNA1**), bearing a nucleobase sequence complementary to that of mature miR-21–5p (5′-TCAACATCAGTCTGATAAGCTA-3′), as well as to a 20-mer oligomer (**PNA2**) used as a negative control bearing the sequence 5′-GTGTAACACGTCCTATACGCC-3'. The resulting four Re-PNA conjugates were characterized and used to target miR-21 in the DU145 prostate cancer cell line. The conjugation with PNA did not perturb the photoluminescence behavior of the organometallic fragments: emission from $^3$MLCT excited states, centered in a range between 580 and 610 nm, was observed, with satisfactory photoluminescence quantum yields ($\Phi$ = ca. 0.03–0.01, in aerated water/acetonitrile solution 1/1). Experiments of cell uptake, performed with living prostate cancer cells showed that the length of the aliphatic linker between the rhenium complex and the PNA sequence, strongly affects the cellular localization.



## 1. Introduction

PNAs are synthetic mimics of natural nucleic acids (DNA and RNA) in which the neutral pseudo-peptide backbone, made of *N*-(2-aminoethyl)glycine units, replaces the negatively charged sugar-phosphate chain of nucleic acids [1]. PNAs show high chemical stability and great resistance to both nucleases and proteases [2], and, most importantly, they are able to recognize and bind in a very high specific and selective manner DNA and RNA [3]. Thanks to these unique features, PNA or their analogs can be designed and synthesized with the aim to recognize and hybridize complementary sequences of mRNA, thereby inhibiting its translation in an antisense strategy. Accordingly, several examples of PNAs were found to be excellent candidates for biosensing applications [4], and antisense or antigene therapy [5–7]. Among them, some PNAs have been shown to be able to alter biological functions of microRNAs, both in vitro and in vivo [8,9].

MicroRNAs (miRNAs) are a class of short non-coding RNAs (ca. 22 nucleotides in length) that play a key role in modulating gene expression at post-transcriptional level [10]. To date, nearly 2.000 miRNAs have been discovered in humans, where they represent one of the most abundant classes of regulatory genes [10,11]. miRNAs have been shown to regulate the life span of messenger RNA by acting as negative regulators of gene expression [11]. MiR-21–5p (has-miR-21–5p, MIMAT0000076, miRBase) has been one of the most studied miRNAs in cancer [10]. It has been found to be widely overexpressed in multiple cancers and though to play a pivotal role in tumorigenesis [10]. In this context, it has been shown that the inhibition of miR-21 by “antisense” oligonucleotides impairs tumor growth and survival, interferes with the invading/migrating capabilities of cancer cells as well as enhances their response to conventional anti-cancer therapies [10]. This evidence has contributed to identify miR-21–5p as an oncomiR and as a suitable therapeutic target for anticancer inventions [10].

Synthetic antisense oligonucleotides (ASOs) are among the most used tools to directly interfere with the expression of oncogenic

* Corresponding author.
*E-mail address:* emanuela.licandro@unimi.it (E. Licandro).

https://doi.org/10.1016/j.jorganchem.2019.02.020
0022-328X/

miRNAs [11]. However, issues dealing with the delivery, stability and specificity of ASOs are still needed to be addressed before nucleic acid-based molecules will be fully exploited as therapeutic agents. Specifically, natural oligonucleotides bearing the classical phosphodiester backbone are susceptible to nuclease-mediated degradation and are characterized by inadequate affinity (*i.e.* low potency) for the target due to binding to similar sequences or to proteins, thus resulting in off-target effects [11]. On the contrary, the use of PNA as third generation antisense oligonucleotides has several advantages as mentioned before.

Unfortunately, unmodified PNAs display very low cellular uptake [12], and this feature still constitutes an important drawback towards the effective use of PNAs in therapy [13–15]. One of the strategy to overcome this problem is the conjugation of PNA to metal complexes [16,17]. Among them, rhenium complexes have been used as PNA carrier. Some examples of mononuclear rhenium-PNA conjugates have been reported in the literature [18–21], but only two of them concerned luminescent complexes [22,23]. $^{188}$Re was selected as the therapeutic radionuclide because of its attractive properties for radiotherapy. It is a generator-based nuclide with a half-life of 17 h and an average β-energy of about 2 MeV. Furthermore, diagnostic $^{99m}$Tc and therapeutic $^{188}$Re form a so-called "matched pair" of radionuclides showing similar coordination properties. Very recently, some $^{99m}$Tc-labelled PNAs have been reported and used in the active tumor pre-targeting approach for therapeutic purposes [24]. Besides these studies, we also reported that dinuclear Re(I) complexes could be used as low-toxicity luminescent tag for PNA labelling [25,26]. These complexes belong to the recently reported family of dinuclear rhenium complexes, which are characterized by two "Re(CO)$_3$" moieties, joined by a substituted bridging diazine ligand and two anionic ancillary ligands. They display intense emission (photoluminescence quantum yields up to 0.5) in the range 550–620 nm, originating from triplet metal-to-ligand-charge transfer excited states $^3$MLCT [27,28]. Due to these interesting properties, some of them have been also successfully used as new, simple, chemically robust, and easy-to-synthetize platform for different carbohydrate ligands, affording novel luminescent glycosylated materials [29,30], and 17α-ethinylestradiol bioconjugates [31].

Some Re-PNA decamers have been synthesized and successfully tested in cell imaging experiments, showing efficient cell uptake in living cells with different kinetics and localization depending on the sequence of PNA [25,26]. The high photoluminescence quantum yield of the dinuclear rhenium complex bound to PNA allows to obtain images at very low concentration with a consequent reduction of the possible cytotoxicity due to the presence of the metal complex.

It is interesting to note that in these dinuclear rhenium complexes, having an idealizing $C_s$ symmetry, the six CO ligands give rise to a peculiar four-band pattern in the IR spectrum [28]. These intense CO absorption IR bands could be employed as probe in vibrational spectroscopy. The development of IR probes is a real challenge in the emerging field of the imaging as it involves no electronic transition and no photobleaching is induced, and many metal-carbonyl complexes are attractive candidates due to their strong absorption in the mid-IR transparency window of the cell (2200–1800 cm$^{-1}$ range) [32–34].

In this paper, we further extend this study by the development of dinuclear Re-based used as imaging agents with two aims: *i)* to examine the relationship between variations in the molecular structure and cellular localization; *ii)* to test the Re-PNA conjugates as therapeutic agents. Herein, we describe the synthesis and the characterization of four novel conjugates (**1**–**4**, Chart 1), in which two selected PNA sequences corresponding to an anti-miR-21 (**PNA1**) and to a negative control oligomer (**PNA2**) were conjugated to dinuclear rhenium complexes **Re-1** and **Re-2** (Chart 1).

The two different dinuclear rhenium complexes **Re-1** and **Re-2**, containing one or two alkyl chains on the diazine ligand utilized in this study, led us to obtain compounds **1, 2** and **3, 4** respectively. This has been done in order to modulate spectroscopic features of conjugates **1**–**4**. Indeed, complex **Re-2**, which contains two alkyl substituents in the 4 and 5 positions of the diazine ring, exhibits a hypsochromically shifted emission with a higher quantum yield and longer lifetime compared to the analogous mono-substituted complex **Re-1**. We have also undertaken preliminary in vitro cell imaging and uptake studies on DU145 prostate cancer cells to assess the potentiality of the new Re-PNA conjugates as antisense tools towards miR-21–5p as oncomiR target.

## 2. Experimental

### 2.1. Materials and instrumentation

Rhenium(I) complexes **Re-1** [25] and **Re-2** [31] were synthesized as previously reported. The PNA oligomers were prepared by solid-phase synthesis (SPS) using the commercially available Boc/Z-protected PNA monomers (ASM Research Chemicals GmbH, Hannover, Germany). Polystyrene beads carrying 4-methylbenzhydrylamine hydrochloride salt groups (MBHA resin, 0.63 mmoL/g) was purchased from VWR International, and it was downloaded to 0.2 mmoL/g with the Boc-thymine PNA monomer for **PNA1**, and with the Boc/Z-guanine PNA monomer for **PNA2**, according to the literature [35]. Polypropylene one-way syringes (4 or 8 mL), used as reaction vessels for the manual SPS, were purchased from Alltech Associates Inc. (Lokeren, Belgium). All reactions on solid-phase were performed using a mechanical shaker at 500 r/min. The reverse-phase RP-HPLC purifications were performed on an Agilent 1200 Series system, equipped with DAD analyzer, using the semi-preparative column DISCOVERY® BIO WIDE PORE C18 (25 cm × 10 mm, 10 μm) at a flow rate of 3 mL/min. Solvent A (0.1% TFA in water) and solvent B (0.1% TFA in acetonitrile) were used in a linear gradient of 10–50% (0–30 min) with detection by UV at 260 and 280 nm. The reverse-phase RP-HPLC analyses of the purified Re-PNA conjugates were performed using the analytical column DISCOVERY® BIO WIDE PORE C18 (15 cm × 4.6 mm, 5 μm) at a flow rate of 1 mL/min. Solvent A (0.1% TFA in water) and solvent B (0.1% TFA in acetonitrile) were used in a linear gradient of 5–100% (0–60 min) with detection by UV at 260 and 280 nm. MALDI-TOF MS spectra were recorded with a Bruker Daltonics Omniflex, equipped with a pulsed nitrogen laser (337 nm), operating in reflector mode (20 kV) with positive polarity, and using sinapinic acid as the matrix.

### 2.2. Synthesis of Re-PNA conjugates

#### 2.2.1. General procedure for the synthesis of resin-supported PNA oligomers *5* and *6*

The resin-supported PNA oligomers **5** and **6** were prepared manually by solid-phase synthesis in a one-way syringe (8 mL) equipped with a frit at the bottom. The MBHA resin (100 mg, 0.2 mmoL/g, 0.02 mmol), downloaded with the proper monomer, was swollen in $CH_2Cl_2$ for 40 min, and the Boc group of the anchored monomer was removed by the treatment with a mixture of TFA/*m*-cresol 95/5 (3 mL, twice for 4 min). The resin beads were then washed with $CH_2Cl_2$, NMP, and then with a solution of DIPEA 5% in $CH_2Cl_2$. In an Eppendorf tube, a solution of DIPEA (10 eq, 0.2 mmol, 35 μL) and the Boc/Z protected monomer (5.3 eq, 0.106 mmol) in NMP was added to a solution of HATU (4.8 eq, 0.096 mmol, 36 mg) in NMP, and the resulting mixture was shaken for 2 min. The activated acid was then transferred to the resin, and shaken for 2 h. The resin was washed with NMP, and treated with a

mixture of $Ac_2O$/pyridine/NMP (1:25:25, twice for 2 min, capping step). The cycle (Boc-deprotection, coupling, and capping) was repeated for each PNA monomer until the completion of the sequence. To verify the oligomerization outcome, some resin beads were washed with TFA, and then shaken with a mixture of TFA/TFMSA/thioanisole/*m*-cresol 6/2/1/1 (300 μL, 1.5 h). The resin was filtered off and washed with TFA. The filtrate was concentrated, and cold $Et_2O$ was added to precipitate the PNA oligomer as a colorless solid. Centrifugation of the slurry gave the product, which was washed with $Et_2O$ and dried to afford the crude PNA oligomers whose MALDI confirmed their identity.

### 2.2.2. General procedure for the synthesis of Re-PNA conjugates *1*–*4*

The resin-supported PNA **5** or **6** (50 mg, 0.2 mmoL/g, 0.01 mmol) was transferred into a one-way syringe (4 mL) equipped with a frit at the bottom, and swollen in $CH_2Cl_2$ for 40 min. The terminal *N*-Boc protecting group was removed by the treatment with a mixture of TFA/*m*-cresol 95/5 (1.5 mL, twice for 4 min), and the resin beads were sequentially washed with $CH_2Cl_2$, NMP, and then with a solution of DIPEA 5% in $CH_2Cl_2$. In an Eppendorf tube, a solution of DIPEA (10 eq, 0.1 mmol, 17 μL) and the rhenium(I) complexes **Re-1** or **Re-2** (5.3 eq, 0.053 mmol) in NMP was added to a solution of HATU (5 eq, 0.05 mmol, 19 mg) in NMP, and the resulting brown mixture was shaken for 2 min. The activated acid was then transferred to the resin, and shaken for 2 h. The resin was thoroughly washed with NMP and $CH_2Cl_2$. The Re-PNA conjugates were then cleaved from the resin using a mixture of TFA/TFMSA/thioanisole/*m*-cresol 6/2/1/1 (1 mL, twice for 1 h). The collected filtrates were first concentrated before being precipitated with cold $Et_2O$. The pale-yellow solid was centrifuged, washed with cold $Et_2O$, and dried under vacuum. The crude Re-PNA conjugates were purified with RP-HPLC, and characterized with MALDI-TOF mass spectrometry.

Re-PNA conjugate **1**: MALDI-TOF MS (*m/z*) calcd for $C_{229}H_{276}Cl_2N_{118}O_{65}Re_2$, 6164.7, found: 6168.0 $[M+H]+$, 6139 $[M-CO]^+$, 6099.1 $[M-2Cl]^+$, 5826.3 $[M-Re(CO)_3Cl_2]^+$, 5555.2 $[M-Re_2(CO)_6Cl_2]^+$. HPLC: $t_R = 24.2$ min.

Re-PNA conjugate **2**: MALDI-TOF MS (*m/z*) calcd for $C_{228}H_{276}Cl_2N_{116}O_{67}Re_2$, 6156.7, found: 6157.7 $[M+H]^+$, 6088.0 $[M + H-2Cl]^+$, 5817.5 $[M + H - Re(CO)_3Cl_2]^+$, 5547.2 $[M + H - Re_2(CO)_6Cl_2]^+$. HPLC: $t_R = 26.5$ min.

Re-PNA conjugate **3**: MALDI-TOF MS (*m/z*) calcd for $C_{234}H_{286}Cl_2N_{116}O_{65}Re_2$, 6234.2, found: 6235.0 $[M+H]^+$, 6207.6 $[M + H-CO]^+$, 6166.9 $[M + H-2Cl]^+$, 5895.0 $[M + H - Re(CO)_3Cl_2]^+$, 5625.5 $[M + H - Re_2(CO)_6Cl_2]^+$. HPLC: $t_R = 27.2$ min.

Re-PNA conjugate **4**: MALDI-TOF MS (*m/z*) calcd for $C_{233}H_{286}Cl_2N_{116}O_{67}Re_2$, 6226.8, found: 6226.8 $[M]^+$, 6199.7 $[M + H-CO]^+$, 6158.2 $[M + H-2Cl]^+$, 6129.2 $[M-CO-2Cl]^+$, 5887.7 $[M + H - Re(CO)_3Cl_2]^+$, 5616.8 $[M-Re_2(CO)_6Cl_2]^+$. HPLC: $t_R = 27.6$ min.

### 2.3. Biological studies

Human prostate cancer cells (DU145) were purchased from the American Type Culture Collection (ATCC® HTB-81, Rockville, MD). Cells were cultured in Roswell Park Memorial Institute 1640 medium (Lonza Milano S.r.l., Treviglio, Italy) supplemented with 10% fetal bovine serum and maintained in a logarithmic growth phase at 37 °C, 5% $CO_2$ in humidified atmosphere. The uptake of Re-PNA conjugates was assessed on DU145 cells seeded in 6-well plates ($1 \times 10^5$ cell/well), incubated at 37 °C for 24 h, and subsequently exposed to 10 μmol $L^{-1}$ of the compounds, diluted at the appropriate working concentration from a 1 mmol $L^{-1}$ stock solution in dimethyl sulfoxide just before use. After a 2-h incubation at 37 °C, cells were washed three times with PBS and incubated for up to 20 h in complete medium. The uptake of Re-complexes was monitored by fluorescence microscopy (Nikon Eclipse E600 microscope, Nikon Instruments S.p.A., Firenze, Italy) on living cells using a Fluorescein-5-isothiocyanate (FITC) filter. Images were acquired by ACT-1 software (Nikon) and processed by Adobe Photoshop Image Reader 7.0.

To assess the expression levels of miR-21, total RNA was isolated using Qiagen RNeasy Mini kit (Qiagen, Hilden, Germany) and digested with 20 U RNase-free DNase. miR-21 expression levels were analysed using TaqMan® microRNA Assay (Thermo Fisher Scientific, MA, USA) specific for the mature forms of miR-21–5p (Assay ID 000397) and mir-21–3p (Assay ID 002438), according to the manufacturer's instruction. Amplifications were run on the 7900HT Fast Real-Time PCR System (Applied Biosystems, CA, USA). Data were analysed by SDS 2.2.2 software (Applied Biosystems). If not otherwise specified, data have been reported as relative quantity (RQ) of miR-21 amounts in treated (100 nmol $L^{-1}$ for 48 h) *vs.* untreated cells (calibrator sample) using the $2^{-\Delta\Delta Ct}$ method [36], where Ct represents the threshold cycle. RNU48 snRNA (P/N 4427975) was used as normaliser during the analysis.

The intracellular fate of the conjugate **3** was evaluated in a time-dependent manner by cell-imaging on DU145 cells ($2 \times 10^5$) grown on glass coverslips and exposed up to 24 h to 10 μmol $L^{-1}$ of the PNA conjugate. At the end of treatments, cells were washed in cold PBS and fixed in 4% formaldehyde/PBS for 15 min. Cell imaging was performed using a confocal laser scanning microscope (TCS SP8 X, Leica Microsystems GmbH, Mannheim, Germany). The internalized compound was excited by a Light Laser with excitation and emission wavelengths of 405 nm and 430–550 nm, respectively. Nuclei were counterstained with the far-red DNA stain DRAQ5™ Fluorescent Probe (Thermo Fisher Scientific), according to the manufacturer's instruction. The images were acquired using a HC PL APO 63X/1.4 oil immersion objective and a pinhole set to 1 Airy unit. Digitalized images were processed by Adobe Photoshop 7.0.1.

## 3. Results and discussion

### 3.1. Design of Re(I)–PNA oligomers *1*–*4*

Two different dinuclear rhenium complexes, namely **Re-1** and **Re-2** (Chart 1) were selected as starting suitable complexes for the synthesis of Re-PNA conjugates **1**–**4**. The two complexes differ in the number and length of alkyl substituents on the diazine ligand: **Re-1** complex bears only an alkyl chain of four carbon atoms, while **Re-2** complex has an additional methyl group adjacent to an alkyl chain of eight carbon atoms. This could bring to tune the photophysical behavior and the cellular uptake of the conjugates **1**–**4**.

From a synthetic point of view, the presence of the terminal carboxylic acid group on both complexes **Re-1** and **Re-2** is fundamental for the covalent attachment of the metal complex to PNA, through an amide bond formation with the terminal free amino group on the PNA sequence.

Complex **Re-1** was already widely used as a luminescent probe for PNA labelling [24,25], while the complex **Re-2** has been conjugated to an antimiR-221 PNA sequence only very recently [33]. We reasoned that **Re-2** could exhibit a hypsochromically shifted emission with a higher quantum yield and longer lifetime compared to the analogous mono-substituted complex **Re-1** [27,28]. Both the diazine ligands were synthesized using the previously reported two-step procedure involving an inverse-electron–demand Diels–Alder cycloaddition reaction between the electron–poor 1,2,4,5-tetrazine and the appropriate functionalized alkynes with $N_2$ loss [38].

Following our previously reported procedure [25,31], complexes **Re-1** and **Re-2** were obtained in good yield as air-stable yellow

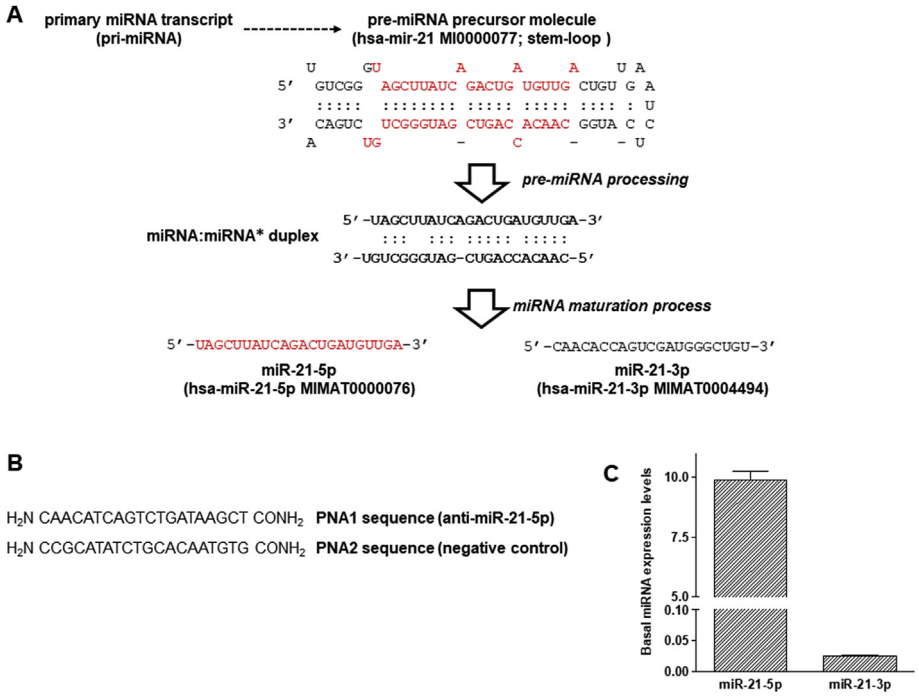


**Fig. 1.** **A**) Schematic representation of miRNA biogenesis. The 100–1000 nucleotide-long primary miRNA transcript (pri-miRNA) is processed within the cell nucleus into a 70 nucleotide-long miRNA precursor molecule (pre-miRNA) that bears a typical hairpin (stem-loop) structure. The pre-miRNA is then exported into the cytoplasm where it undergoes a processing into a miRNA:miRNA* duplex which eventually leads to the mature, active form of the miRNA during a maturation process involving the miRISC complex. The reported miRNA sequences and accession numbers are from miRBase 22.1 (http://www.mirbase.org/); **B**) Chemical structure of PNA sequences; **C**) Quantification of basal (endogenous) miR-21–5p and -3p expression levels in DU145 cells by real-time RT-PCR. Data have been reported as $2^{-\Delta Ct}$ and represent mean value ± s.d. from at least three independent experiments.

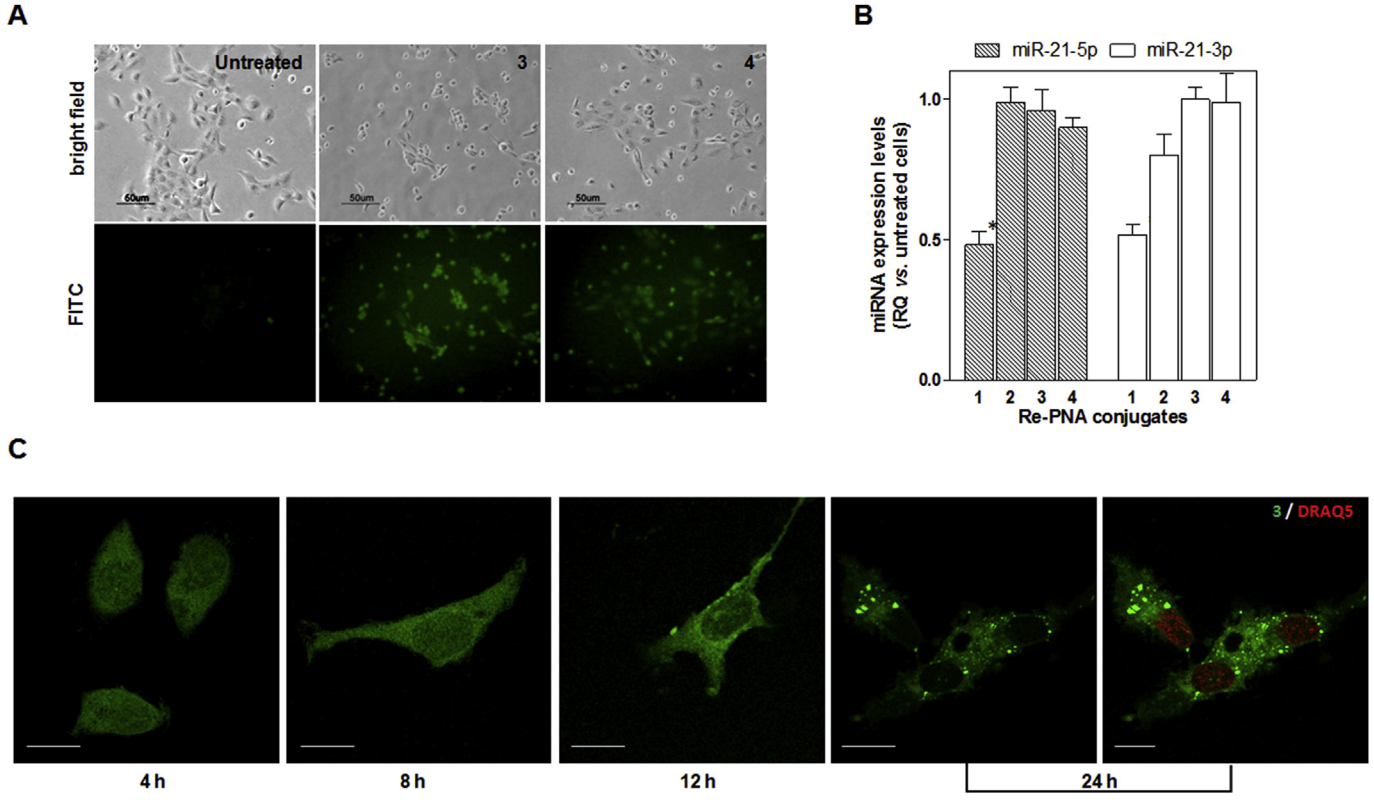


**Fig. 2.** A) Representative photomicrographs showing the internalization of Re-PNA conjugates **3** and **4** assessed in living DU145 cells by fluorescence microscopy. Images were captured 20 h after 2 h exposure to 10 μmol $L^{-1}$ of conjugates. Untreated cells at the same time point were used as control for PNA internalization. The upper panels show bright field images. Magnification × 10; Scale bar: 50 μm; B) Quantification of miR-21–5p (dashed bars) and -3p (white bars) expression levels in DU145 cells treated for 48 h with 100 nmol $L^{-1}$ of Re-conjugates **1**–**4**. Data have been reported as RQ and represent mean values ± s.d. from at least three independent experiments. $^{*}P < 0.05$; $^{**}P < 0.01$; C) Representative photomicrographs showing the kinetics of **3** internalization assessed by confocal microscopy in DU145 cells exposed for 2 h to 10 μmol $L^{-1}$ of the conjugate. Nuclei in the images captured at 24 h were counterstained with the far-red DNA stain DRAQ5™ Fluorescent Probe, according to the manufacturer's instruction. Magnification × 63; Scale bar: 5 μm. (For interpretation of the references to color in this figure legend, the reader is referred to the Web version of this article.)

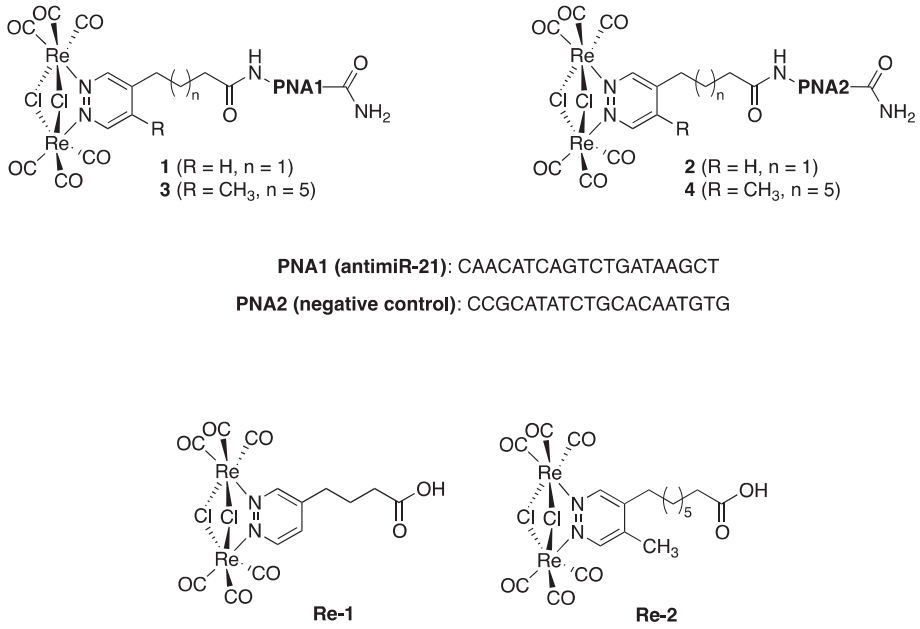


**Chart 1.** Structure of Re-PNA conjugates **1**–**4** and Re(I) complexes **Re-1** and **Re-2** used in this study.

solids by refluxing $[Re(CO)_5Cl]$ with 0.5 equivalents of the corresponding 1,2-diazine in toluene solution.

These two complexes have been conjugated to two different PNA sequences to give the four biorganometallic conjugates **1**–**4** (Chart 1), able to target oncomiR-21 as therapeutic target in the DU145 prostate cancer cell line. In particular, we designed and synthetized a 20-mer oligomer (**PNA1**) bearing a nucleobase sequence complementary to that of mature miR-21–5p (5′-TCAACATCAGTCTGATAAGCTA-3′, Fig. 1B [39]), as well as a 20-mer oligomer (**PNA2**) used as a negative control PNA and bearing a sequence (5′-GTGTAACACGTCCTATACGCC-3′) with no significant homology with any known transcript within the human genome (Fig. 1B).

### 3.2. Synthesis of Re(I)–PNA oligomers *1*–*4*

At the onset of this study, the two resin-supported PNA oligomers **5** and **6** (Scheme 1) were synthesized manually on methylbenzhydryl amine (MBHA) polystyrene resin using standard Boc/Z-based solid-phase synthesis (SPS) [35], and the commercially available Boc/Z-protected PNA monomers, in which the terminal amino group on the backbone is protected with a *tert*-butyloxycarbonyl (Boc) group, while the amino groups on the nucleobases are protected as benzyloxycarbonyl (Z) derivatives. To verify the efficiency of the oligomerization process, a small amount of both resins **5** and **6** was treated with a mixture of TFA/TFMSA/thioanisole/*m*-cresol, and the presence of cleaved oligomers antimiR-21 PNA1 and negative control PNA2 was confirmed by MALDI-TOF MS analyses (see Figures S1 and S2, Appendix A-Supplementary Data).

Having secured good access to the resin-supported PNA **5** and **6**, we initially focused our attention on the synthesis of Re-PNA conjugates **1** and **2** using the complex **Re-1** under experimental conditions very similar to those optimized by our group to efficiently conjugate **Re-1** complex to PNA decamers [26].

More in detail, as reported in Scheme 1, the *N*-terminal Boc protecting groups of **5** and **6** was removed with a mixture of TFA/*m*-cresol, and the corresponding free amine groups of resin-supported PNA oligomers were reacted with the carboxylic group of the **Re-1** complex in the presence of HATU as condensing agent and DIPEA as base in NMP for 2 h, to form the amide bond.

The final cleavage of both Re–PNAs conjugates from the resin, under standard acidic conditions, provided pale-yellow crude products **1** and **2**, which were purified by RP-HPLC using a semi-preparative column C18. The purity and identity of purified oligomers **1** and **2** were evaluated by analytical HPLC and MALDI-TOF MS analysis (see Figures S3–S6, Appendix A-Supplementary Data). The same synthetic approach was also used for the synthesis of Re-PNA conjugates **3** and **4**, using in this case the preformed complex **Re-2**. Also in this case, the conjugation of **Re-2** complex to **PNA1** and **PNA2** on the solid support was found to be successful, affording, after the final cleavage and further HPLC purification, the conjugates **3** and **4** as pale-yellow solids, whose identity and purity were confirmed by MALDI and analytical RP-HPLC (see Figures S7–S10,

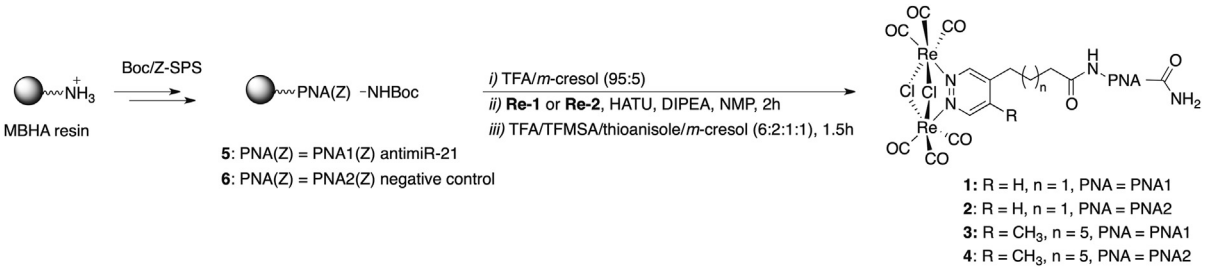


**Scheme 1.** Synthesis of Re-PNA conjugates **1**–**4**.

Appendix A-Supplementary Data).

It should be noted that, as previously observed for **Re-1** complex, **Re-2** complex also displays a good stability toward strong acidic conditions required by the Boc/Z strategy for the cleavage of the PNA from the MBHA resin, and the simultaneous deprotection of exocyclic amino groups of nucleobases.

### 3.3. Photophysical properties

The photoluminescence in the whole family of dinuclear Re-diazine complexes originates from $d\pi(Re)-\pi^*$(diazine) triplet metal-ligand-to-ligand charge transfer excited states ($^3$MLLCT) [28,40]. Several arguments support this attribution: the solvent effect on the energy and on the intensity of the emission, the quenching of the emission in the presence of $O_2$ and the effect of the diazine substituent on the emission energy [28]. In particular, the position of the emission is not affected by the length of the alkyl substituents, but only by their number. Accordingly, complexes featuring diazine ligands containing two alkyl substituents in the 4 and 5 positions displayed absorption and emission bands blue-shifted with respect to the mono substituted complexes. Indeed, the second electro-donating alkyl chain on the diazine ligand increases the energy level of the LUMO, raising in this way the HOMO–LUMO gap and therefore the energy of the MLCT excited states [27]. It is interesting to note that thanks to the presence of the aliphatic chain that hamper the conjugation between biomolecules, such as PNA [25,26,37], carbohydrates [29,30], and estradiol moiety [31] and the Re-diazine moiety, the photophysical properties of bioconjugates are analogous to that of Re-diazine complex alone. In the specific case of Re-PNA conjugates, neither the length nor the nature of the PNA oligomer modify the photophysical behavior of the conjugates. Actually, all the **Re-1**-PNA conjugates elsewhere described display, in air equilibrated water/acetonitrile 1/1 solution, photophysical features very similar to those of the parent **Re-1** ($\lambda_{em}$ in the range 607–611 nm, $\Phi = 0.012–0.016$) [25,26]. Moreover, we have recently reported the photophysical properties of a **Re-2**-PNA conjugate containing an antimiR-221 PNA sequence [37]. In this case, upon optical excitation in air equilibrated water/acetonitrile 1/1 solution, both **Re-2** complex and **Re-2-**PNA show a broad emission centered at 578 nm ($\Phi = 0.03$), almost 30 nm blue-shifted with respect to the emission of the corresponding **Re-1** and **Re-1**-PNA derivatives previously reported. This is in agreement with the presence of the two alkyl substituents on the diazine ligand and the higher photoluminescence quantum yield fairly follows the Energy Gap Law [41]. For these reasons, we have not here performed the photophysical characterization of the PNA conjugates **1**–**4** in that, on the basis of the above considerations, we are confident that these conjugates exhibit photophysical properties analogous to that of **Re-1** and **Re-2**.

### 3.4. Biological characterizations

In order to examine the potential applicability of the Re-PNA conjugates **1**–**4** in living cells, cell-imaging studies were performed using the commercially available prostate cancer (DU145) cell line. Fluorescence microscopy analysis carried out on living cells 20 h after the incubation of cells at 37 °C for 2 h in the presence of 5 μmol $L^{-1}$ of the conjugates revealed an intense and homogenously distributed green fluorescent signal (Fig. 2A). This evidence clearly indicates that both **3** and **4** conjugates were spontaneously and efficiently taken up by DU145 cells, in keeping with our previous observations showing that other PNAs conjugated to **Re-1** are easily detected within cells [25,26].

The potential of Re-PNA conjugates for miR-21 inhibition was hence assessed in DU145 prostate cancer cells, which are characterized by elevated levels of endogenous miR-21–5p compared to other PCa cell lines [39] and show little amounts of the respective miRNA on the -3p arm (miR-21–3p) of the precursor molecule (MI0000077, miRBase; Fig. 1C). Specifically, the amounts of endogenous miR-21–5p were evaluated by real-time RT-PCR after a 48 h exposure of DU145 cells to equimolar amounts (100 nM) of **1**–**4** conjugates. Results showed that **1**-treated cells were characterized by a significant depletion (~50%; $P < 0.01$, Fig. 2B) of mature miR-21–5p amounts with respect to cells exposed to the **2**-negative control conjugate ($0.48 \pm 0.04$ and $0.99 \pm 0.05$ relative quantity (RQ) *vs.* untreated cells, respectively). Notably, a significant reduction ($P < 0.05$) in the amounts of endogenous miR-21–3p was also observed in cells exposed to **1** with respect to cells treated with an equimolar amount of **2** (RQ: $0.52 \pm 0.04$ and $0.80 \pm 0.07$, respectively; Fig. 2B). Conversely, **3**-treated cells did not show significant modulation in the expression levels of both miR-21–5p and miR-21–3p in comparison to cells exposed to an equimolar amount of the **4**-negative control conjugate (Fig. 2B) as well as with respect to untreated cells. This evidence would suggest that conjugate **1** likely acts as a miR-21 inhibitor by impinging on the processing of pre-miR-21 precursor molecule (Fig. 1A) [42]. Importantly, no cytotoxicity was observed in cells treated with up to 2 μmol $L^{-1}$ each of the four Re-conjugates (data not shown).

Our previous fluorescence microscopy analysis showed that conjugate **3** was efficiently taken-up by living cells (Fig. 2A), thus indicating that the unsuccessful modulation in the expression levels of both miR-21–5p and -3p was not attributable to its poor internalization. This evidence was further confirmed by confocal microscopy analyses showing that 4 h after 2 h incubation at 37 °C in the presence of **3** (10 μmol $L^{-1}$), the conjugate was quickly taken-up by cells and mainly localized within the cytoplasm (Fig. 2C). However, 20 h later the cells were profoundly characterized by the appearance of highly fluorescent granules (Fig. 2C). This observation would suggest that the permanence of the conjugate within the cytoplasm may lead to the formation of PNA aggregates, likely due to the presence of a long aliphatic chain in the **Re-2** complex, that impinge on the miRNA inhibitory activity of the conjugate. Alternatively, it can be also hypothesized that the molecule may be targeted to the endosome/lysosome compartment for possible degradation, as previously observed in the same cell line exposed to high concentration of a naked PNA targeting human telomerase [43].

## 4. Conclusions

Fluorescence microscopy is one of the most widely used techniques for the visualization of the cells and for studying biological processes. Different fluorophores have been developed for this purpose and, among them luminescent transition-metal complexes have recently received an increasing interest in this field, even if this area is still in its infancy. Therefore, this work, which describes the development of dinuclear Re-based organometallic complexes used as imaging agents, clearly indicate that: i) the Re-PNA conjugates are easily taken up by living cells thus showing that the Re(I) complexes are indeed useful tools for the intracellular delivery of PNA; ii) Re complexes may be exploited as fluorescent probes to track the cell uptake of biologically relevant molecules. However, our attempts to carefully design probes more performing from the photophysical point of view, introducing two aliphatic substituents on the diazine ligand, afford not trivial variations in uptake and localization of the corresponding conjugates. The possible formation of intracellular aggregates or the targeting of the Re-PNA conjugates **3** and **4**, to endosome/lysosome compartment are detrimental for exploiting their biological activity.

On the contrary, experiments performed using conjugate **1** revealed that the PNA may act as miRNA inhibitor, likely due to their capability to interfere with cytoplasmic processing of the miRNA precursor molecules, opening the way to use the Re-PNA derivatives as efficient antisense molecules in cancer diseases.

## Acknowledgments

The authors are thankful to Dr. P. Casalini (Microscopy facility, Fondazione IRCCS Istituto Nazionale dei Tumori di Milano) for her helpful support in cell imaging analyses by confocal microscopy. S.C., M. P. and E. L. acknowledge the Ministero dell'Istruzione, dell'Università e della Ricerca for financing the national project PRIN 2009, prot. 20093N774P, title: "Molecular recognition of microRNA (miR) by modified PNA: from structure to activity".

## Appendix A. Supplementary data

Supplementary data to this article can be found online at https://doi.org/10.1016/j.jorganchem.2019.02.020.

## References

[1] P.E. Nielsen, M. Egholm, R.H. Berg, O. Buchardt, Sequence-selective recognition of DNA by strand displacement with a thymine-substituted polyamide, Science 254 (1991) 1497–1500. https://doi.org/10.1126/science.1962210.
[2] S. Karkare, D. Bhatnagar, Promising nucleic acid analogs and mimics: characteristic features and applications of PNA, LNA, and morpholino, Appl. Microbiol. Biotechnol. 71 (2006) 575–586. https://doi.org/10.1007/s00253-006-0434-2.
[3] M. Egholm, O. Buchardt, L. Christensen, C. Behrens, S.M. Freier, D.A. Driver, R.H. Berg, S.K. Kim, B. Norden, P.E. Nielsen, PNA hybridizes to complementary oligonucleotides obeying the Watson–Crick hydrogen-bonding rules, Nature 365 (1993) 566–568. https://doi.org/10.1038/365566a0.
[4] C. Briones, M. Moreno, Applications of peptide nucleic acids (PNAs) and locked nucleic acids (LNAs) in biosensor development, Anal. Bioanal. Chem. 402 (2012) 3071–3089. https://doi.org/10.1007/s00216-012-5742-z.
[5] A. Gupta, A. Mishra, N. Puri, Peptide nucleic acids: advanced tools for biomedical applications, J. Biotechnol. 259 (2017) 148–159. https://doi.org/10.1016/j.jbiotec.2017.07.026.
[6] C. Sharma, S.K. Awasthi, Versatility of peptide nucleic acids (PNAs): role in chemical biology, drug discovery, and origins of life, Chem. Biol. Drug Des. 89 (2017) 16–37. https://doi.org/10.1111/cbdd.12833.
[7] V.L. Marin, S. Roy, B.A. Armitage, Recent advances in the development of peptide nucleic acid as a gene-targeted drug, Expert Opin. Biol. Ther. 4 (2004) 337–348. https://doi.org/10.1517/14712598.4.3.337.
[8] R. Gambari, E. Fabbri, M. Borgatti, I. Lampronti, A. Finotti, E. Brognara, N. Bianchi, A. Manicardi, R. Marchelli, R. Corradini, Targeting microRNAs involved in human diseases: a novel approach for modification of gene expression and drug development, Biochem. Pharmacol. 82 (2011) 1416–1429. https://doi.org/https://doi.org/10.1016/j.bcp.2011.08.007.
[9] D.A. Braasch, D.R. Corey, Novel antisense and peptide nucleic acid strategies for controlling gene expression, Biochemistry 41 (2002) 4503–4510. https://doi.org/10.1021/bi0122112.
[10] P. Marzia, F. Marco, G. Paolo, Z. Nadia, MicroRNAs and the response of prostate cancer to anti-cancer drugs, Curr. Drug Targets 17 (2016) 257–265. https://doi.org/10.2174/1389450116666150316223341.
[11] S. Francesca, G. Paolo, C.-R. Graziella, Z. Nadia, F. Marco, MicroRNA-dependent regulation of telomere maintenance mechanisms: a field as much unexplored as potentially promising, Curr. Pharmaceut. Des. 20 (2014) 6404–6421. https://doi.org/10.2174/1381612820666140630095918.
[12] U. Koppelhus, S.K. Awasthi, V. Zachar, H.U. Holst, P. Ebbesen, P.E. Nielsen, Cell-dependent differential cellular uptake of PNA, peptides, and PNA-peptide conjugates, antisense and, Nucleic Acid Drug Dev 12 (2002) 51–63. https://doi.org/10.1089/108729002760070795.
[13] A. Gupta, R. Bahal, M. Gupta, P.M. Glazer, W.M. Saltzman, Nanotechnology for delivery of peptide nucleic acids (PNAs), J. Control. Release 240 (2016) 302–311. https://doi.org/10.1016/j.jconrel.2016.01.005.
[14] E. Rozners, Recent advances in chemical modification of peptide nucleic acids, J. Nucleic Acids 8 (2012), 2012, https://doi.org/10.1155/2012/518162.
[15] P.E. Nielsen, Addressing the challenges of cellular delivery and bioavailability of peptide nucleic acids (PNA), Q. Rev. Biophys. 38 (2006) 345–350. https://doi.org/10.1017/S0033583506004148.
[16] R. Krämer, A. Mokhir, Metal complex derivatives of peptide nucleic acids (PNA), in: A. Sigel, H. Sigel, R.K.O. Sigel (Eds.), Interplay between Metal Ions and Nucleic Acids, Springer, Dordrecht, 2012, pp. 319–340. https://doi.org/10.1007/978-94-007-2172-2.
[17] G. Gasser, A.M. Sosniak, N. Metzler-Nolte, Metal-containing peptide nucleic acid conjugates, Dalton Trans. 40 (2011) 7061–7076. https://doi.org/10.1039/C0DT01706J.
[18] M. Patra, G. Gasser, D. Bobukhov, K. Merz, A.V. Shtemenko, N. Metzler-Nolte, Sequential insertion of three different organometallics into a versatile building block containing a PNA backbone, Dalton Trans. 39 (2010) 5617–5619. https://doi.org/10.1039/C003598J.
[19] C. Xavier, C. Giannini, S. Dall'Angelo, L. Gano, S. Maiorana, R. Alberto, I. Santos, Synthesis, characterization, and evaluation of a novel $^{99m}Tc(CO)_3$ pyrazolyl conjugate of a peptide nucleic acid sequence, J. Biol. Inorg. Chem. 13 (2008) 1335–1344. https://doi.org/10.1007/s00775-008-0419-y.
[20] K.A. Stephenson, S.R. Banerjee, T. Besanger, O.O. Sogbein, M.K. Levadala, N. McFarlane, J.A. Lemon, D.R. Boreham, K.P. Maresca, J.D. Brennan, J.W. Babich, J. Zubieta, J.F. Valliant, Bridging the gap between in vitro and in vivo Imaging: isostructural Re and $^{99m}Tc$ complexes for correlating fluorescence and radioimaging studies, J. Am. Chem. Soc. 126 (2004) 8598–8599. https://doi.org/10.1021/ja047751b.
[21] K.A. Stephenson, J. Zubieta, S.R. Banerjee, M.K. Levadala, L. Taggart, L. Ryan, N. McFarlane, D.R. Boreham, K.P. Maresca, J.W. Babich, J.F. Valliant, A new strategy for the preparation of peptide-targeted radiopharmaceuticals based on an fmoc-lysine-derived single amino acid chelate (SAAC). Automated solid-phase synthesis, NMR characterization, and in vitro screening of fMLF(SAAC)G and fMLF[$(SAAC-Re(CO)_3)^+$]G, Bioconjug. Chem. 15 (2004) 128–136. https://doi.org/10.1021/bc034128s.
[22] G. Gasser, S. Neumann, I. Ott, M. Seitz, R. Heumann, N. Metzler-Nolte, Preparation and biological evaluation of di-hetero-organometallic-containing PNA bioconjugates, Eur. J. Inorg. Chem. 2011 (2011) 5471–5478. https://doi.org/10.1002/ejic.201100734.
[23] G. Gasser, A. Pinto, S. Neumann, A.M. Sosniak, M. Seitz, K. Merz, R. Heumann, N. Metzler-Nolte, Synthesis, characterisation and bioimaging of a fluorescent rhenium-containing PNA bioconjugate, Dalton Trans. 41 (2012) 2304–2313. https://doi.org/10.1039/C2DT12114J.
[24] M. Patra, K. Zarschler, H.-J. Pietzsch, H. Stephan, G. Gasser, New insights into the pretargeting approach to image and treat tumors, Chem. Soc. Rev. 45 (2016) 6415–6431. https://doi.org/10.1039/c5cs00784d.
[25] E. Ferri, D. Donghi, M. Panigati, G. Prencipe, L. D'Alfonso, I. Zanoni, C. Baldoli, S. Maiorana, G. D'Alfonso, E. Licandro, Luminescent conjugates between dinuclear rhenium(I) complexes and peptide nucleic acids (PNA) for cell imaging and DNA targeting, Chem. Commun. 46 (2010) 6255–6257. https://doi.org/10.1039/C0CC00450B.
[26] C. Mari, M. Panigati, L. D'Alfonso, I. Zanoni, D. Donghi, L. Sironi, M. Collini, S. Maiorana, C. Baldoli, G. D'Alfonso, E. Licandro, Luminescent conjugates between dinuclear rhenium complexes and peptide nucleic acids (PNA): synthesis, photophysical characterization, and cell uptake, Organometallics 31 (2012) 5918–5928. https://doi.org/10.1021/om3004515.
[27] M. Mauro, E.Q. Procopio, Y. Sun, C.-H. Chien, D. Donghi, M. Panigati, P. Mercandelli, P. Mussini, G. D'Alfonso, L. De Cola, Highly emitting neutral dinuclear rhenium complexes as phosphorescent dopants for electroluminescent devices, Adv. Funct. Mater. 19 (2009) 2607–2614. https://doi.org/10.1002/adfm.200900744.
[28] M. Panigati, M. Mauro, D. Donghi, P. Mercandelli, P. Mussini, L. De Cola, G. D'Alfonso, Luminescent dinuclear rhenium(I) complexes containing bridging 1,2-diazine ligands: photophysical properties and application, Coord. Chem. Rev. 256 (2012) 1621–1643. https://doi.org/https://doi.org/10.1016/j.ccr.2012.03.006.
[29] A. Palmioli, A. Aliprandi, D. Septiadi, M. Mauro, A. Bernardi, L. De Cola, M. Panigati, Glyco-functionalized dinuclear rhenium(i) complexes for cell imaging, Org. Biomol. Chem. 15 (2017) 1686–1699. https://doi.org/10.1039/C6OB02559E.
[30] A. Palmioli, M. Panigati, A. Bernardi, Glycodendron–rhenium complexes as luminescent probes for lectin sensing, Org. Biomol. Chem. 16 (2018) 8413–8419. https://doi.org/10.1039/C8OB01838C.
[31] M. Proverbio, E. Quartapelle Procopio, M. Panigati, S. Mercurio, R. Pennati, M. Ascagni, R. Leone, C. La Porta, M. Sugni, Luminescent conjugates between dinuclear rhenium complexes and 17α-ethynylestradiol: synthesis, photophysical characterization, and cell imaging, Org. Biomol. Chem. 17 (2019) 509–518. https://doi.org/10.1039/C8OB02472C.
[32] S. Clède, C. Policar, Metal-carbonyl units for vibrational and luminescent imaging: towards multimodality, Chem. Eur J. 21 (2015) 942–958. https://doi.org/10.1002/chem.201404600.
[33] M. Salmain, A. Vessières, Organometallic complexes as tracers in non-isotopic immunoassay, in: G. Jaouen (Ed.), Bioorganometallics: Biomolecules, Labelling, Medicine, Wiley-VCH, Weinheim, 2006, pp. 263–302. https://doi.org/10.1002/3527607692.
[34] S. Clède, N. Cowan, F. Lambert, H.C. Bertrand, R. Rubbiani, M. Patra, J. Hesse, C. Sandt, N. Trcera, G. Gasser, J. Keiser, C. Policar, Bimodal X-ray and infrared imaging of an organometallic derivative of praziquantel in *Schistosoma mansoni*, Chembiochem 17 (2016) 1004–1007. https://doi.org/10.1002/cbic.201500688.
[35] G. Prencipe, S. Maiorana, P. Verderio, M. Colombo, P. Fermo, E. Caneva, D. Prosperi, E. Licandro, Magnetic peptide nucleic acids for DNA targeting, Chem. Commun. (2009) 6017–6019. https://doi.org/10.1039/B911449A.
[36] K.J. Livak, T.D. Schmittgen, Analysis of relative gene expression data using real-time quantitative PCR and the 2−ΔΔCT method, Methods 25 (2001) 402–408. https://doi.org/10.1006/meth.2001.1262.
[37] M. Panigati, S. Cauteruccio, E. Licandro, A. Finotti, R. Milani, E. Brognara, R. Gambari, (in preparation).

[38] J. Sauer, D.K. Heldmann, J. Hetzenegger, J. Krauthan, H. Sichert, J. Schuster, 1,2,4,5-Tetrazine: synthesis and reactivity in [4+2] cycloadditions, Eur. J. Org. Chem. 1998 (1998) 2885–2896. https://doi.org/10.1002/(SICI)1099-0690(199812)1998:12<2885::AID-EJOC2885>3.0.CO;2-L.

[39] M. Folini, P. Gandellini, N. Longoni, V. Profumo, M. Callari, M. Pennati, M. Colecchia, R. Supino, S. Veneroni, R. Salvioni, R. Valdagni, M.G. Daidone, N. Zaffaroni, miR-21: an oncomir on strike in prostate cancer, Mol. Canc. 9 (2010) 12. https://doi.org/10.1186/1476-4598-9-12.

[40] D. Donghi, G. D'Alfonso, M. Mauro, M. Panigati, P. Mercandelli, A. Sironi, P. Mussini, L. D'Alfonso, A new class of luminescent tricarbonyl rhenium(I) complexes containing bridging 1,2-diazine ligands: electrochemical, photophysical, and computational characterization, Inorg. Chem. 47 (2008) 4243–4255. https://doi.org/10.1021/ic7023692.

[41] J.V. Caspar, T.J. Meyer, Application of the energy gap Law to nonradiative, excited-state decay, J. Phys. Chem. 87 (1983) 952–957.

[42] C. Avitabile, E. Fabbri, N. Bianchi, R. Gambari, A. Romanelli, Inhibition of miRNA maturation by peptide nucleic acids, in: C. Arenz (Ed.), miRNA Maturation: Methods and Protocols, Humana Press, Totowa, NJ, 2014, pp. 157–164.

[43] M. Folini, K. Berg, E. Millo, R. Villa, L. Prasmickaite, M.G. Daidone, U. Benatti, N. Zaffaroni, Photochemical internalization of a peptide nucleic acid targeting the catalytic subunit of human telomerase, Cancer Res. 63 (2003) 3490–3494.